International Journal of Minerals, Metallurgy and Materials
Accepted manuscript, https://doi.org/10.1007/s12613-020-2023-2

Invited original article

Effect of flash processing on recrystallization behavior and mechanical performance of cold rolled IF steel

Peng-yu Wen[1,2)], Jian-sheng Han[1)], Hai-wen Luo[1,2)] and Xin-ping Mao[1)].*

1) State Key Laboratory of Advanced Metallurgy, University of Science and Technology Beijing, Beijing 100083, China

2) Department of Ferrous Metallurgy, University of Science and Technology Beijing, Beijing 100083, China

ABSTRACT

Flash processing (FP) has attracted considerable attentions due to its high efficiency, economic advantage and extraordinary opportunity to improve mechanical properties. In this paper, influences of FP on the recrystallization (REX) behavior and mechanical performance of a cold-rolled IF steel were investigated. Both the single-stage FP with the heating rates of 200 and 500°C/s and the two-stage FP, including the first preheating to 400°C at 5°C/s and then to peak temperatures at 200°C/s, were performed on a thermomechanical simulator. In comparison with the continuous annealing (CA), the single-stage FPs could effectively refine the recrystallized grain sizes and produce a similar or even sharper γ (ND//{111}) texture component; in particular, the one at 500°C/s led to the increase of yield strength by about 23.2% and the similar ductility. In contrast, the two-stage FP resulted in not

* Corresponding author: Haiwen Luo E-mail: luohaiwen@ustb.edu.cn (H. Luo)

only higher REX temperature but also a certain grain refinement because stored strain energy as the driving force for REX was largely consumed during preheating; furthermore, both the stronger {110}<110> and weaker γ texture components appear in the two-stage FP and is believed to be responsible for the early necking and deteriorated ductility.

Keywords: Flash processing; interstitial-free steel; recrystallization; mechanical properties; texture

1. Introduction

Interstitial-free (IF) steel is an irreplaceable advanced high strength steel (AHSS) for automotive, in which the interstitial elements C and N atoms are scavenged by the addition of Ti or Nb elements [1]. It's well known that this steel possesses excellent formability and especially superior deep drawability due to the existence of strong γ (ND//{111}) fiber recrystallization (REX) texture [2-4], and it has been extensively used in the outer shells of cars [5]. In the past decade, considerable efforts have been made to achieve the extremely low contents of C and N by the optimized metallurgical processing [6, 7] for further improving drawability; whilst a stronger and ductile IF steel is now in demand for automobile due to the light weight restraint. For an example, heterogeneous microstructures were formed by some extra mechanical deformation processes [8-10] that could manufacture stronger IF steel due to the mechanical incompatibility between the gradient layers. Nevertheless, all of

them face a great difficulty on the commercialization.

Flash processing (FP) has emerged as one of the most promising methods to develop stronger AHSS steel via grain refinement in an unprecedented high efficiency [11]. However, the scale-up of FP to an industrial product size may cause the large distortion of thin flat product due to the induced high thermal stress; thus, a preheating stage is often included to minimize the temperature gradient [12]. There are a lot of controversies on how the heating rate and preheating stage could affect the REX and mechanical properties of cold-rolled IF steel, leading to no unanimous explanation until now. The key point is whether the increased heating rate could bring higher REX temperature and result in grain refinement. Atkinson et al. [13, 14] measured a lower hardness on low-carbon steels after the FP with higher heating rate due to lower onset temperature for REX. However, more recent researches suggested that the higher heating rate could raise the REX onset temperature in both ultralow/low carbon steels [15, 16] and IF steel [17, 18]. Moreover, Reis at al. [19] observed a saturation of grain refinement in a severely deformed IF steel when the heating rate is beyond 1000°C/s. In this paper, a received commercial cold rolled IF steel was subjected to two different FPs. One is direct heating to the target peak temperature at either 200°C/s or 500°C/s; the other is to include a preheating stage before the ultrafast heating to the peak temperature. The REX behavior during the two FPs and the resultant mechanical performance were then studied to resolve this dispute.

2. Experimental

A 0.8-mm thick sheet of IF commercial cold-rolled steel sheet, having the chemical composition of 0.0015 C-0.01 Si-0.1 Mn-0.03 Al-0.02 Ti (all in weight percent, wt%) and subjected to 60% cold rolled reduction in thickness, was received from steel industry. Specimens for FP were cut from the sheet and have the dimension of 20 mm × 100 mm with the length parallel to the rolling direction. Some of them were directly heated at 200°C/s or 500°C/s to the designed different peak temperatures and then water quenched immediately, *i.e.* the single-stage FP. Others were subjected to the two-stage FP, *i.e.* they were firstly preheated to 400°C at 5°C/s and to different peak temperatures at 200°C/s. On the purpose of tracing REX kinetics under both FPs, some peak temperatures are chosen at an interval of 25°C between 700°C to 800°C and at an interval of 15°C between 840°C and 870°C, as shown in Fig. 1. In particular, the single-stage FPs with the peak temperatures at both 715°C and 725°C and the two-stage FP at 730°C were also performed as they all lead to about 50% REXed fraction. For comparison, one was heated in a box furnace to 870°C for 5 min to simulate the continuous annealing (CA) process. All the FPs were performed on a Gleeble-1500 thermomechanical simulator, on which a temperature distribution with the deviation less than 5°C could be achieved in the 30 mm-length zone at the middle of specimen according to the previous temperature measurements using three thermocouples. The above processes for the heating to 870°C are then termed 200-870, 500-870 for the single-stage FP, P870 for two-stage FP and CA870 for CA process respectively.

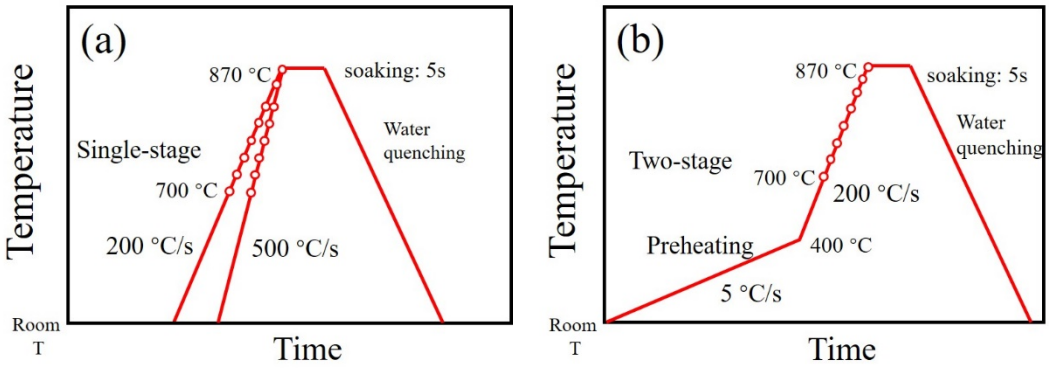

Fig. 1. Schematic illustration for the different flash processing employed in this study. (a) the single-stage FP; (b) the two-stage FP with the imposed preheating stage.

The evolution of micro-hardness on the samples during FP, which were deliberately interrupted during different FPs to 870 °C (see Fig. 1), was traced using a micro-hardness tester (FM300) under the loading of 200 g with a dwell time of 10 s. Uniaxial tensile tests were conducted at the strain rate of 6.67×10^{-4} s^{-1} on a WDW-200D tensile testing machine, using the ASTM-E8/E8M standard samples with the gauge length of 25 mm.

The microstructures before and after these heat treatments were first examined by optical microscopy (OM). The samples for OM were etched in 4% nitric alcohol for 10 s after the standard mechanical polishing. Electron back-scattered diffraction (EBSD option of Scanning Auger Nanoprobe, PHI710, with angular accuracy of 0.1°) measurements were performed at the accelerated voltage of 20 kV with the step size of 0.5 μm on the samples that had been subjected to electropolishing in 20% alcohol perchlorate. EBSD examinations were made on the plane perpendicular to the transverse direction (TD) with the area of about 0.03 mm^2 near the half-thickness

region of specimen. The EBSD data were all processed by EDAX OIM software using the clean-up function of grain dilation type with the parameters of 5° grain tolerance angle, 2 level of minimum grain size and single iteration. Orientation distribution function (ODF) was calculated with the step size of 5º. Kernel average misorientation (KAM) mapping was made by selecting the 1st nearest neighbor and the upper cut of limit less than 5° misorientation. In addition, low-angle and high-angle grain boundaries are defined as the boundary misorientation angles lower and higher than 15º respectively.

3. Results

3.1 Initial cold-rolled microstructure

The received cold-rolled microstructure was examined at the section perpendicular to the transverse direction near the half thickness, which is shown in Fig. 2. Shear bands were observed in between the layers of elongated grains (Fig. 2a) due to the severe deformation and formed via dislocation glide and rigid-body rotation [20]. They are mostly located in γ -fiber (ND//{111}) grains exhibited blue color and a small fraction in α-fiber (RD//<110>) that may be represented by the orange and purple color [21] in the orientation map of Fig. 2a, and deviate from the longitudinal rolling direction by 20-40°. This is consistent with the previous finding that γ-fiber is more easily formed than α -fiber at the initial stage of cold rolling [22]. Please note just a few {110}<uvw> grains also appearing in the cold-rolled microstructure component, as marked in green color in Fig. 2a. Comparison of ODF at φ_2=45º (Fig.

2b) and the ideal positions of α texture in BCC steel (Fig. 2c) also reveals both γ-fiber and α -fiber; and the strongest texture components are {112}<110> and {111}<011> with intensity values more than 8.88 mrd (multiples of random density).

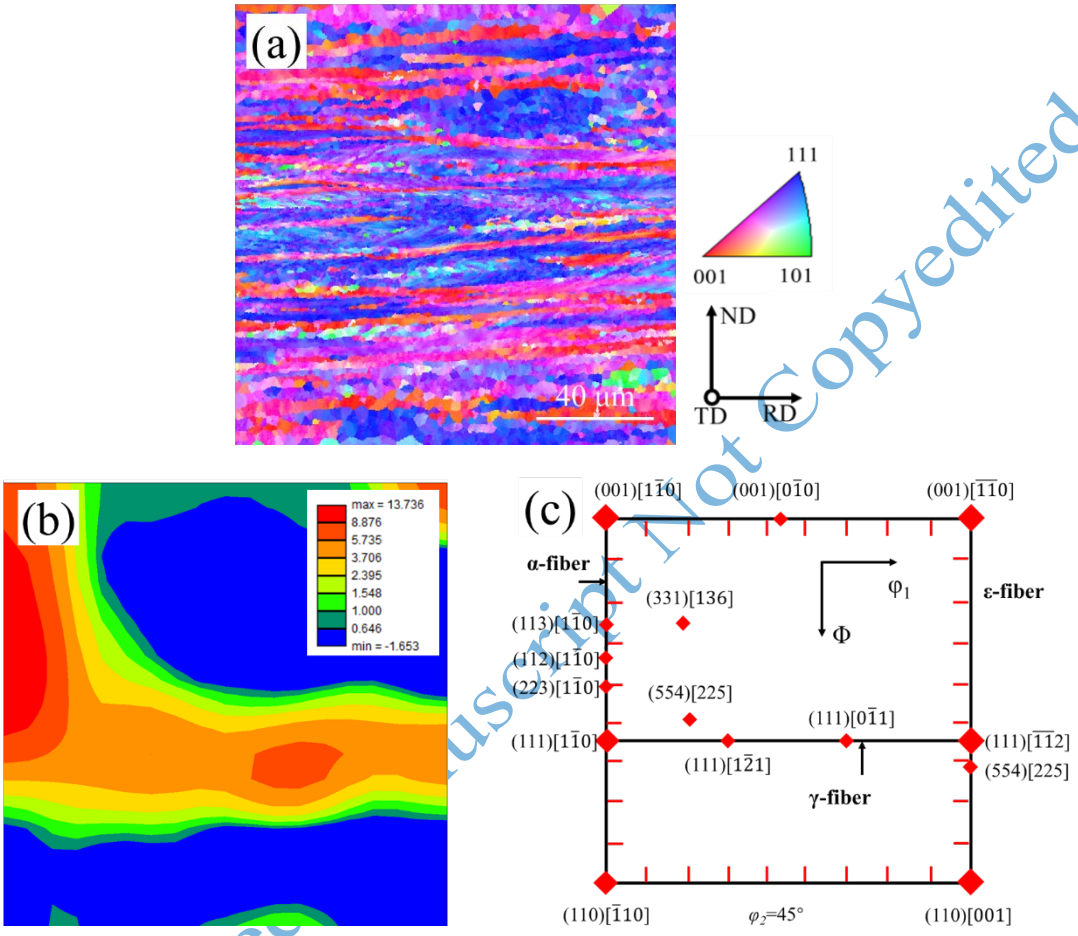

Fig. 2. EBSD normal direction-inverse pole figure (ND-IPF) for orientation mapping (a), ODF images at φ_2=45° for the cold-rolled IF steel (b) and the ideal positions of some important BCC texture components at φ_2=45° section of Euler space (c).

3.2 Hardness evolution and tensile properties

The micro-hardness on the samples heated to different peak temperatures at the same rate was measured to trace the REX kinetics. The average value was taken from

ten measurements for each sample. The REXed fraction, X_T, is calculated by [23, 24]

$$X_T = \frac{H_{\max} - H_T}{H_{\max} - H_{\min}} \quad (1)$$

where H_{max} is hardness of cold rolled IF steel in the as-received state, H_{min} the hardness in fully recrystallized state, and H_T is the hardness on the sample heated to different peak temperatures before the full REX.

Fig. 3a shows the measured REXed fractions as a function of peak temperature for the different FP routines together with the correspondent fittings with high correlative coefficients. The temperatures for 50% and 100% REXed fractions under the different FPs could be then precisely determined from these fitting curves. It can be seen that the increase of heating rate just led to slightly higher temperature for the onset of REX; in contrast, the preheating stage strongly delayed REX so that the temperature for 90% REXed fraction increased from 720°C to 750°C. The grain size distributions in the fully REXed samples, measured on about 500 grains, are shown in Fig. 3b. It can be clearly seen that all the FP routines led to larger fraction of fine grains and then smaller average grain size than the CA process when all specimens were heated to 870°C. In particular, the increase of heating rate from 200°C/s to 500°C/s made negligible effect on grain refinement; whilst the preheating stage produced the finest grain size.

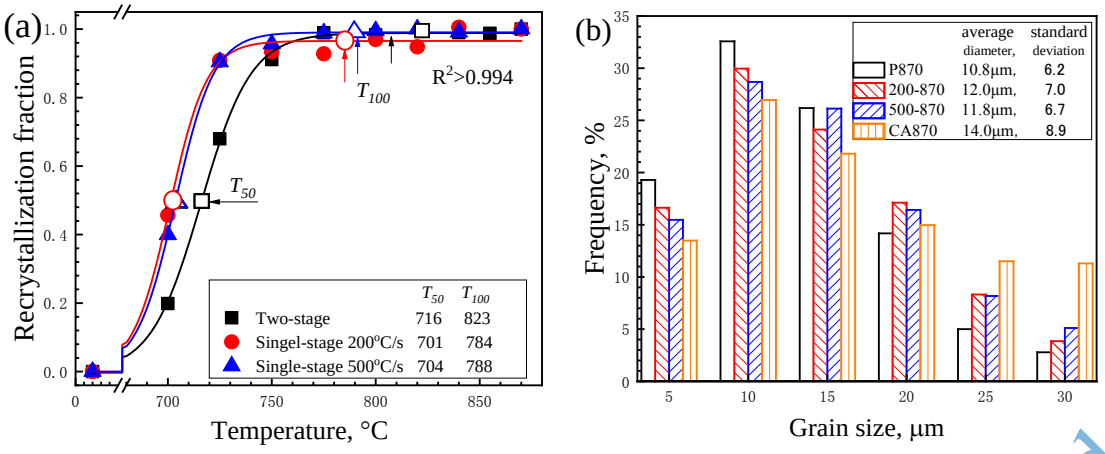

Fig. 3. The recrystallized fraction as a function of peak temperatures for the different heating processes (a), and the resultant grain size distribution (b) in the fully recrystallized specimens after heating to 870° C.

The temperatures for the 50% (T_{50}) and fully REXed fractions (T_{100}) in the different heating processes could be calculated in Fig. 3a. The heating rate in the single-stage FP made negligible influence on REX temperature, but the preheating clearly led to the increase of T_{50} by about 15°C and T_{100} by about 40 °C respectively, as listed in Fig. 3a.

The measured tensile properties are given in Fig. 4, which reveals a clear tendency that the increasing peak temperature could lead to the decrease in both s yield strength (YS) and ultimate tensile strength (UTS), and the increase in both total elongation (TE) and uniform elongation (UE). This is apparently because higher temperature promotes recovery and REX as commonly expected [8, 25-27]. Compared to the CA process, the single-stage FP to 870°C at 200°C/s and 500°C/s resulted in the increases of YS by about 14% and 23% respectively. The best mechanical properties were achieved in the 500-870 specimen, including the UTS value of 299 MPa, YS 147 MPa and TE 43%. This demonstrates the great advantage

of FP on further improving mechanical properties of cold rolled steel sheet in addition to its unprecedented high efficiency. In contrast, the two-stage FP including the preheating stage led to higher strength as expected but much lower ductility, see Fig. 4, and the latter is out of expectation.

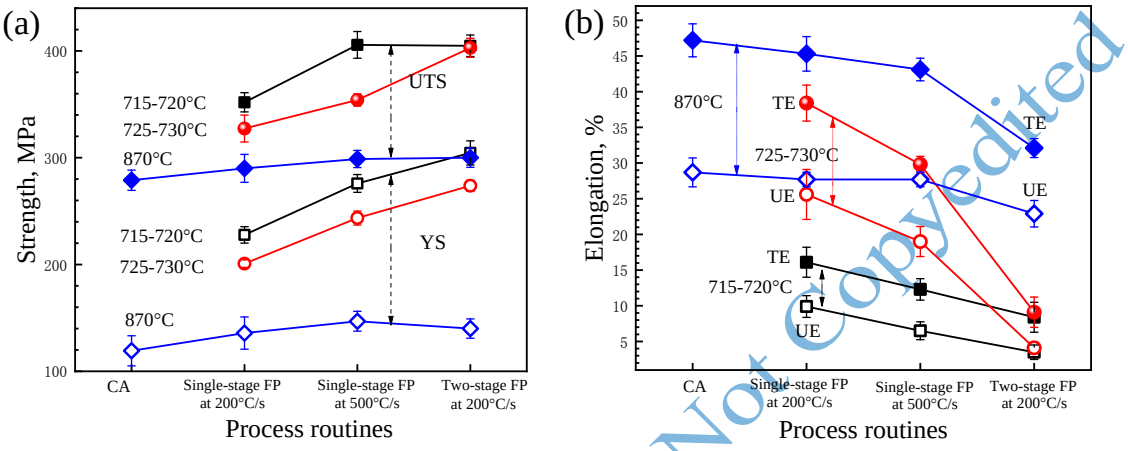

Fig. 4. Engineering properties of IF steel after heating with varied routines that contain single-stage FP at 200 and 500°C/s, two-stage FP at 200°C/s and CA process: (a) yield strength (YS) and ultimate tensile strength (UTS), and (b) total elongation (TE) and uniform elongation (UE) change with varied process routines.

3.2 Microstructural and textural examinations

Extensive EBSD characterizations were made to examine the microstructural evolution during the different FP processes. Fig. 5 shows the proceeding REX during both the single-stage and two-stage FPs. These REXed grains boundaries are high angled [28] and marked with black color in this case. When the cold rolled IF steel was directly heated to 725°C at either 200°C/s or 500°C, it produced a much larger REX fraction than that heated to 715°C (See Fig. 5a through 5h), suggesting that 725°C should be the critical temperature for most of cold deformed microstructure

being recrystallized. According to the ND-IPF maps in Fig. 5, most REXed grains were located in γ -fiber, which is independent of the processing routine. Moreover, higher heating rate clearly retarded REX; particularly, the introduced preheating stage showed stronger inhibition on REX, leading to much fewer REX nuclei found in P720. It's also noted that partial REXed grains have the orientation around {110} fiber (in green color), see dashed line marked in Fig. 5l, suggesting that the preheating stage should affect the nuclei orientation for the REX. These evolutions are consistent with the recrystallization kinetics as depicted in Fig. 3a.

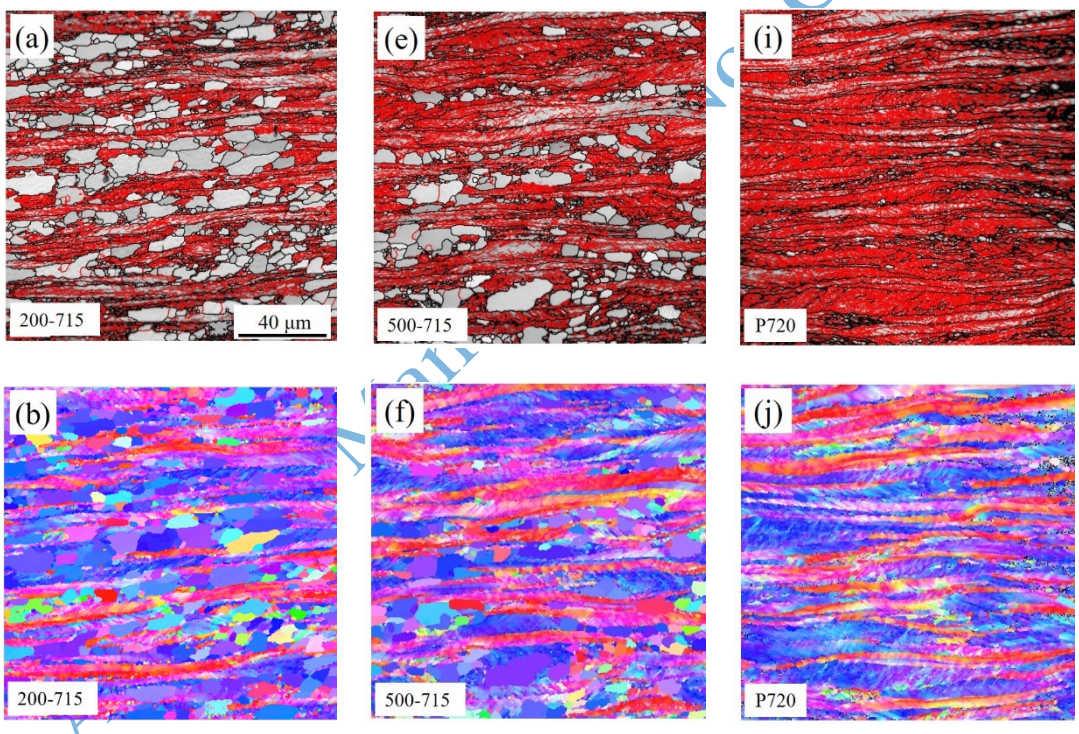

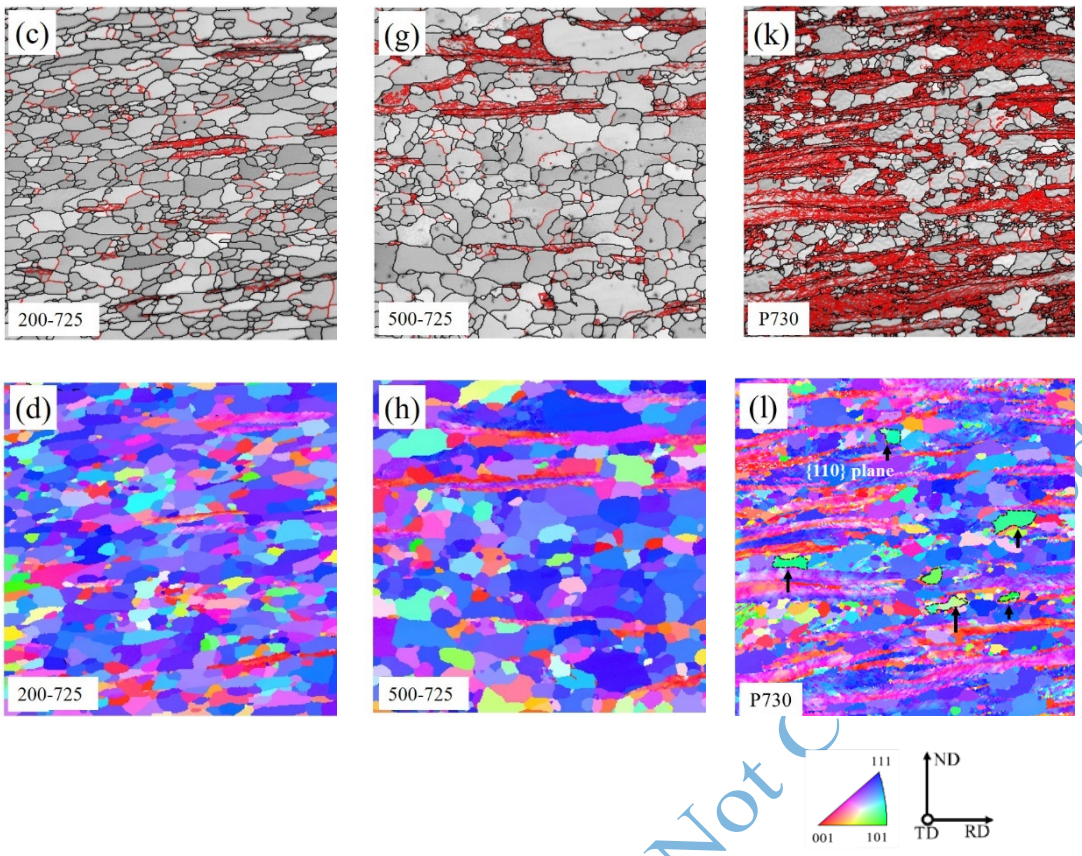

Fig. 5. EBSD image quality ((IQ) overlapped with boundary mapping (GB) and ND-IPF on the cold IF steel heated to various peak temperatures by the different processes. (a, b) 200-715; (c, d) 200-725; (e, f) 500-715; (g, h) 500-725; (i, j) P720; (k,l) P730. {110} fiber is marked by dashed line in (l); low-angle grain boundaries having 0-15° misorientation are in red and high-angle grain boundaries over 15° are in black in IQ+GB maps.

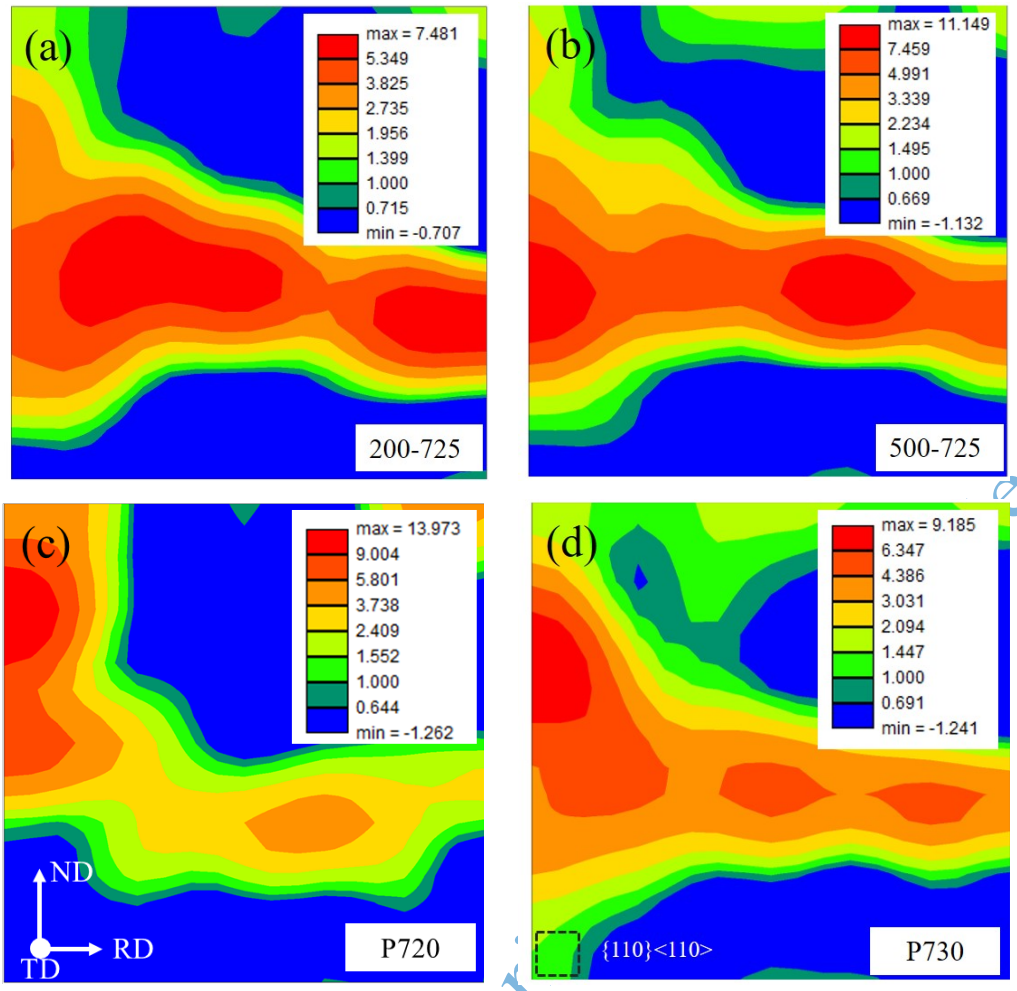

Fig. 6. ODF maps at φ_2=45° of partial REXed microstructures in 200-725 (a), 500-725(b), P720 (c) and P730 (d) specimens. {110}<110> orientation is marked by dashed box in (d).

Fig. 6 is ODF mapping on the partially REXed specimens that were heated to the similar temperatures with the different processes. Faster heating should lead to greater suppression on REX, leading to higher intensity of cold rolled texture retained in 500-725 than 200-725. In 200-725 sample, the γ texture is concentrated on {554}<225> and {111}<112> with the largest value of 7.48 mrd. Fig. 6c and d show that the texture components in P720 and P730 are similar to the cold -rolled texture; moreover, the increase of peak temperature from 720 to 730 leads to stronger γ -fiber in P730. In particular some grains in P730 have an orientation near {110}<110>,

which was not found in the cold rolled and single-stage FP specimens shown in both Figs. 2 and 6. This indicates that the introduced preheating in the two-stage FP may change the nuclei orientation for REX.

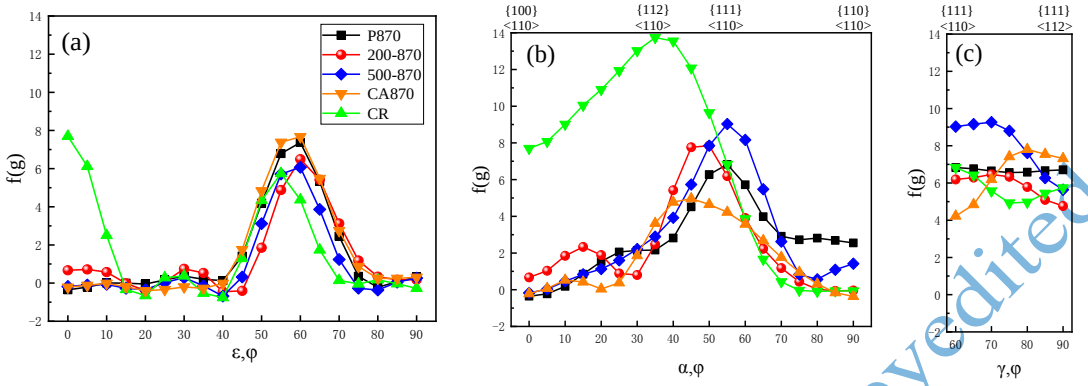

Fig. 7. Orientation density of (a) ε fiber, (b) α fiber, and (c) γ fiber texture in the cold rolled IF steel heated to 870 ºC by the different processes.

Fig. 7 shows the orientation intensity near ε-fiber (TD//<110>), α-fiber (RD//<110>), and γ fiber (ND//{111}) in both cold-rolled and fully recrystallized microstructures, the latter was achieved by the heating to 870°C via the different routines. After the REX, the dominant α texture component in the cold rolled microstructure vanished while γ-fiber was enhanced, suggesting that some α-fiber grains may be consumed by the formation of γ-fiber grains during REX. The rapidest heating in the single-stage FP led to the strongest γ fiber formed in 500-870 and centered on {111}<110>; whilst both the imposed preheating or lower heating rate led to weaker γ fiber having a wider spreading orientation. The strongest {110}<110> component was found in P870, presumably resulting from the imposed preheating stage, which is in a good agreement with the micro-texture results on P730 in Figs. 5l and 6d.

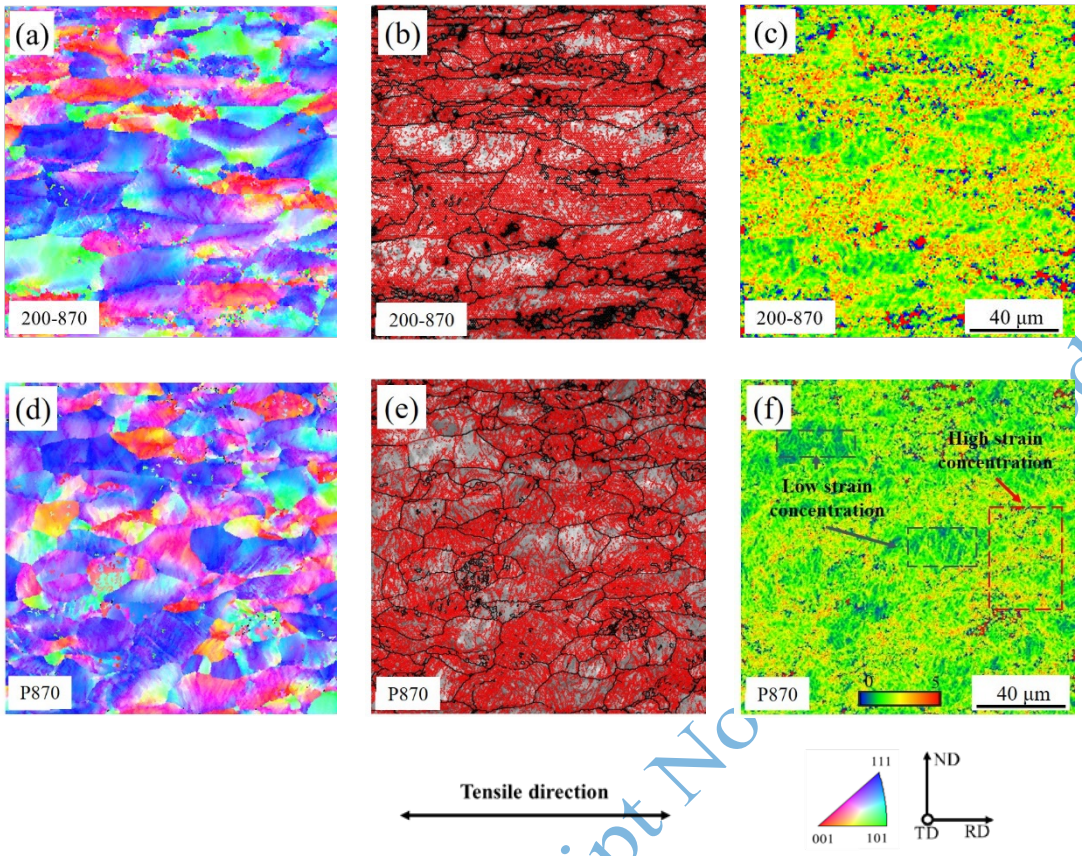

Fig. 8. Comparison of EBSD microstructures in the center of the longitudinal section after the tensile fracture of 200-870 and P870. (a, d) ND-IPF figure; (b, e) IQ+GB map; (c, f) Kernel Average Misorientation (KAM) map. (a, b, c) 200-870; (d, e, f) 870. Red and dark blue color in (f) represents high and low strain concentration respectively. Low-angle grain boundaries having 0-15° misorientation are in red and high-angle grain boundaries over 15° are in black in IQ+GB maps.

Both the microstructures and textures after the tensile fracture of 200-870 and P870 specimens were examined. Higher density of GNDs developed in 200-870 with the corresponding higher strain concentration than P870, see Fig. 8a through 8f, primarily because the former experienced a larger fracture strain. It can be seen from the KAM maps of Figs. 8c and 8f that many {111}<uvw> oriented grain interiors were subjected to a relatively low strain localization.

4. Discussion

4.1 Influence of heating rate and preheating stage on REX

The above stated experimental results can be summarized as follows. First, compared to the traditional CA process, all the FPs produce finer grains, clearly due to much short time available for the grain growth; second, the increase of heating rate from 200°C/s to 500°C/s has little influence on the REX temperature but the introduction of preheating in the two-stage FP significantly raises the REX temperature, further refines recrystallized grains and produces stronger {110}<110> texture component than the single-stage FP.

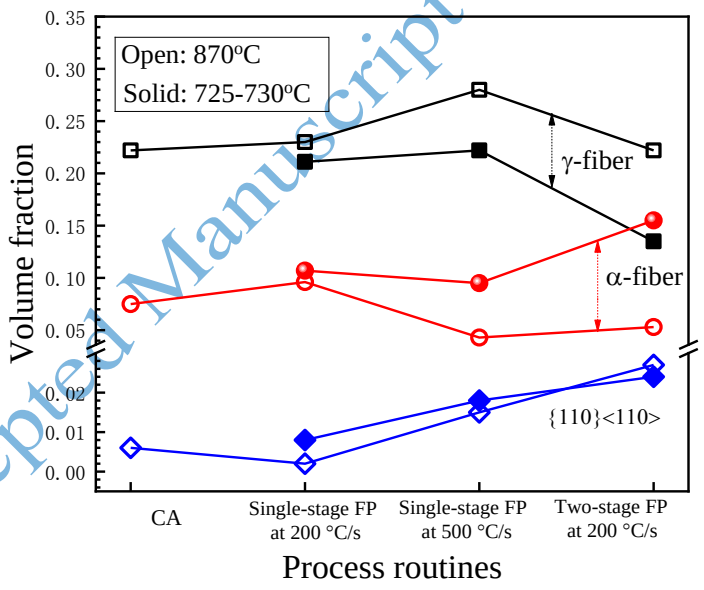

Fig. 9. The fractions of α-fiber, γ-fiber and {100} <110> with the 15° deviation after the different heating processes. α-fiber includes {112}<110>, {113}<110>, {114}<110>, {445}<110>, {223}<110>; γ-fiber includes {111}<112>, {111}<123>, {111}<134>, {111}<110>, {554}<225>.

The preheating should promote the active recovery before REX; as a

consequence, the stored strain energy was reduced greatly, leading to lower driving force for the subsequent REX and the rise of REX temperature.

The fractions of α-fiber and γ-fiber, both of which include the components defined in Ref. [29, 30] and the {110}<110> texture were measured with deviation less than 15°. Their results are shown in Fig. 9, clearly revealing that larger fraction of γ fiber are formed at the expense of α-fiber. This is actually consistent with the previous extensive results on the REX annealing of cold-rolled IF steel [31, 32]. The most popular theory for the formation of REX texture is either oriented nucleation [33, 34] or selective growth [35]. The oriented nucleation assumes that strain-free REX nuclei are prevalent in grains with particular orientation; whilst the selective growth theory is established on the observation of preferred growth of grains with a specific orientation from a randomly oriented array of nuclei [35].

Despite it's widely reported that early nucleation preferentially occurs around {110} and {111} orientations with relatively high stored strain energy [3, 33, 36, 37]. Both experimental and modeling results for texture change during the static REX of IF steel indicated that {110}<110> fiber is prominent in nucleation texture but would be gradually eliminated in the growth texture due to its very limited growth capability [32]. According to the texture modeling results, the nucleation probability increases with increased stored strain energy of components whilst the growth probability of particular orientation is determined by the inclination angle between the axis <*uvw*>, which relates the nucleus to the matrix, and the <110> axis which is perpendicular to the most active slip system in ferrite [32]. Thus, the calculated growth probability

along α fiber is highest at the angle of 20° but gradually decreases with higher angle up to 90 ° (along the left axis of Fig. 2c) that is near {110}<110>, as shown in Fig. 8 of Ref. [32]. This phenomenon is consistent with the observation that the {110}<110> fraction decreases with the increase of peak temperature under all FPs except for the two-stage one, see Fig. 9.

Surprisingly, it now appears that the employed two-stage FP could produce about 2.7vol% {110}<110> texture components in P870 sample; even the single-stage FP at 500 °C/s produces about 1.5vol% {110}<110> texture and the γ texture up to 28vol% in 500-870, see Fig. 9. This probably results from much shorter duration for recrystallization due to faster heating or the great elevation of recrystallization temperature, compared to the conventional CA process; thus the prominent nucleation texture of {110}<110> could not be eliminated in time and still remain even after REX. This may be confirmed by some {110} oriented grains remaining after the partial REX at lower temperature, as displayed in Fig. 5l. Moreover, the sharpened γ texture might relate to the reservation of higher stored strain energy due to such a rapid heating, which could provide larger driving force for the extensive seeding of high energy γ orientated grains.

4.2 The effect of heating rate and preheating stage on mechanical performance

As aforementioned, the comparison of CA-870, 200-870 and 500-870 indicate that the FP can manufacture stronger and ductile cold-rolled IF steel in an unprecedented efficiency. However, the introduced preheating stage during FP, aiming

at relieving the thermal stress for a precise shape control, would slightly increase strength but unavoidably deteriorate ductility. The elevation of strength can be ascribed to the refinement of recrystallized grains, which, however cannot be ascribed to the plastic deterioration.

It has been revealed that during the deformation, the dislocation movement can be subdivided into three steps: *i)*. extensive formation of cell walls which are consisted of abundant geometry necessary dislocations (GNDs), lying at an angle of 20-40° with the rolling direction; *ii)*. at intermediate strain, the substructures are broken up followed by the onset of new slip activity, the latter could produce micro-shear bands; and *iii)*. the complete lamellar dislocation boundary morphology is formed at high strains [22]. Generally, the slip in BCC structure are easily proceeding on the close packed planes, i.e. {110}, {112}, and {123} planes. In addition, Li *et al.* [22] found that dislocation walls compromised by GNDs were mostly parallel to the {110} plane and the micro-shear bands parallel to the {112} plane in cold-rolled IF steel. Thus, he suggested that slip might proceed firstly from {110} plane then into {112} plane at intermediate strain, and the establishment of new slip system in an existing dislocation structure might lead to strain localization, which caused a significant loss in ductility.

Nevertheless, Rollett *et al.* [38] found that the choice of slip plane in bcc metals was affected by the temperature of deformation. At temperatures below $T_m/4$ (melting temperature), slip at {112} occurs; between $T_m/4$ and $T_m/2$, slip at {110} is favored and at temperatures above $T_m/2$ {123} is preferred. This means that the deformation

of {110} texture is difficult when tensile deformation is carried out at room temperature. In this case, Fig. 9 indicates that the highest volume fraction of {110}<110> orientation is obtained in P870 sample, which should contribute to the observed decrease of ductility due to severe strain localization (see Fig. 8f) that leads to an earlier necking than other specimens. Moreover, it's generally believed that the stronger the γ (ND//{111}) texture is, the stronger anti-thinning ability can be achieved, which could simultaneously benefit the deep drawing property. In contrast, even though about 1.5vol% {110}<110> fiber is also formed in 500-870, the ductility is rarely affected that might be due to its sharper γ texture components, which has great resistance to the early strain localization [39, 40].

5. Conclusions

Both single-stage and two-stage flash processing (FP) have been employed to anneal the commercial cold-rolled IF steel, and the following conclusions can be drawn:

(1) In comparison with the continuous annealing (CA) at 870°C, both single and two-stage FPs could refine the recrystallized grain sizes, thus leading to an elevation of yield strength over 13.9% and 23.2% and the decent ductility at the rates of 200°C/s and 500 °C/s, respectively.

(2) The imposed preheating stage in the two-stage FP could raise the REX temperature more than the increase of heating rate in the single-stage FP; however, it deteriorates ductility. Compared to the single-stage FP, the two-stage FP produced

larger fraction of {110}<110> and smaller fraction of γ texture, which might favor the strain localization and then lead to earlier necking and deteriorated ductility.

(3) In summary, the single-stage FP, rather than the two-stage FP including preheating, is then recommended for the future industrial production of cold rolled IF steel due to its high production efficiency and the significantly improved mechanical properties.

Acknowledgement

The authors acknowledge the continuous financial supports from National Natural Science Foundation of China (Nos. 51861135302 and 51831002) and Fundamental Research Funds for the Central Universities (No. FRF-TP-18-002C2).

References

[1] R.K. Ray, J.J. Jonas, and R.E. Hook, Cold rolling and annealing textures in low carbon and extra low carbon steels, *Metall. Rev.*, 39(1994), No. 4, p. 129.

[2] I. Samajdar, B. Verlinden, L. Kestens, and P.V. Houtte, Physical parameters related to the developments of recrystallization textures in an ultra low carbon steel, *Acta Mater.*, 47(1998), No. 1, p. 55.

[3] Y. Hayakawa and J.A. Szpunar, Modeling of texture development during recrystallization of interstitial free steel, *Acta Mater.*, 45(1997), No.6, p. 2425.

[4] C.Y. Qiu, L. Li, L.L. Hao, J.G. Wang, X. Zhou, and Y.L. Kang, Effect of continuous annealing temperature on microstructure and properties of ferritic rolled

interstitial-free steel, *Int. J. Miner. Metall. Mater.*, 25(2018), No. 5, p. 536.

[5] Y.F. Shen, W.Y. Xue, Y.D. Wang, Y.D. Liu, and L. Zuo, Tensile behaviors of IF steel with different cold-rolling reductions, *Mater. Sci. Eng. A*, 496(2008), No. 1, p. 383.

[6] R. Wang, Y.P. Bao, Z.J. Yan, D.Z. Li, and Y. Kang, Comparison between the surface defects caused by Al_2O_3 and TiN inclusions in interstitial-free steel auto sheets, *Int. J.*

Miner. Metall. Mater., 26(2019), No. 2, p. 38.

[7] R. Wang, Y.P. Bao, Y.H. Li, Z.J. Yan, D.Z. Li, and Y. Kang, Influence of metallurgical processing parameters on defects in cold-rolled steel sheet caused by inclusions, I *Int. J. Miner. Metall. Mater.*, 26(2019), No. 4, p. 56.

[8] L. Zhang, Z. Chen, Y.H. Wang, G. Ma, T. Huang, G. Wu, and D.J. Jensen, Fabricating interstitial-free steel with simultaneous high strength and good ductility with homogeneous layer and lamella structure, *Scripta Mater.*, 141(2017), p. 111.

[9] M. Yang, Y. Pan, F. Yuan, Y.T. Zhu, and X. Wu, Back stress strengthening and strain hardening in gradient structure, *Mater. Res. Lett.*, 4(2016), No. 3, p. 145.

[10] R. Saha and R.K. Ray, Formation of nano- to ultrafine grains in a severely cold rolled interstitial free steel, *Mater. Sci. Eng. A*, 459(2007), No. 1, p. 223.

[11] Q.G. Meng, J. Li, and H. Zheng, High-efficiency fast-heating annealing of a cold-rolled dual-phase steel, *Mater. Design*, 58(2014), p. 194.

[12] F.C. Cerda, C. Goulas, I. Sabirov, L. Kestens, and R. Petrov, The effect of the pre-heating stage on the microstructure and texture of a cold rolled FeCMnAlSi steel

under conventional and ultrafast heating, *Mater. Charact.*, 130(2017), p. 188.

[13] M. Atkinson, Bifurcation of thermal restoration processes in deformed iron and steel, *Mater. Sci. Eng. A*, 262(1999), No. 1-2, p. 33.

[14] M. Atkinson, On the credibility of ultra rapid annealing, *Mater. Sci. Eng. A*, 354(2003), No. 1-2, p. 40.

[15] D. Muljono, M. Ferry, and D. Dunne, Influence of heating rate on anisothermal recrystallization in low and ultra-low carbon steels, *Mater. Sci. Eng. A*, 303(2001), No. 1-2, p. 90.

[16] M. Ferry, D. Muljono, and D.P. Dunne, Recrystallization kinetics of low and ultra low carbon steels during high-rate annealing, *ISIJ. Int.*, 41(2001), No. 9, p. 1053.

[17] L. Kestens, A.C.C. Reis, W. Kaluba, and Y. Houbaert, Grain refinement and texture change in interstitial free steels after severe rolling and ultra-short annealing, [in] *Proceedings of the Mater. Sci. Forum*, 2004, p. 287.

[18] F.M. Castro Cerda, F. Vercruysse, T.N. Minh, L. Kestens, A. Monsalve, and R. Petrov, The effect of heating rate on the recrystallization behavior in cold rolled ultra low carbon steel, *Steel Res. Int.*, 88(2017), No. 1, p. 1066351.

[19] A.C.C. Reis, L. Bracke, R. Petrov, W. Kaluba, and L. Kestens, Grain refinement and texture change in interstitial free steels after severe rolling and ultra-short annealing, *ISIJ Int.*, 43(2003), No. 8, p. 1260.

[20] Q. Chen, M. Quadir, and B. Duggan, Shear band formation in IF steel during cold rolling at medium reduction levels, *Philos. Mag.*, 86(2006), No. 23, p. 1478.

[21] Z.Y. Hou, Y.B Xu, and D. Wu, Recrystallization of ultra-low carbon steel sheet

after ultra-rapid annealing, *Acta Metall. Sin.*, 48(2012), No. 9, p. 1057.

[22] B. Li, A. Godfrey, Q.G. Meng, Q. Liu, and N. Hansen, Microstructural evolution of IF-steel during cold rolling, *Acta Mater.*, 52(2004), No. 4, p. 1069.

[23] S. Dziaszyk, E. Payton, F. Friedel, V. Marx, and G. Eggeler, On the characterization of recrystallized fraction using electron backscatter diffraction: A direct comparison to local hardness in an IF steel using nanoindentation, *Mater. Sci. Eng. A*, 527(2010), No. 29-30, p. 7854.

[24] J. Bocos, E. Novillo, M. Petite, A. Iza-Mendia, and I. Gutierrez, Aspects of orientation-dependent grain growth in extra-low carbon and interstitial-free steels during continuous annealing, *Metall. Mater. Trans. A*, 34(2003), No. 3, p. 1341.

[25] A. Smith, H.W. Luo, D.N. Hanlon, J. Sietsma, and S.V. Der Zwaag, Recovery processes in the ferrite phase in C-Mn steel, *ISIJ. Int.*, 44(2004), No. 7, p. 1188.

[26] H.W. Luo, J. Sietsma, and S.V. Der Zwaag, Effect of inhomogeneous deformation on the recrystallization kinetics of deformed metals, *ISIJ. Int.*, 44(2004), No. 11, p. 1931.

[27] H.W. Luo, Comments on “Austenite stability of ultrafine-grained transformation-induced plasticity steel with Mn partitioning” by S. Lee, S.J. Lee and B.C. De Cooman, *Scripta Mater.*, 65 (2011), No. 10, p. 225.

[28] F. Yang, H.W. Luo, E. Pu, S. Zhang, and H. Dong, On the characteristics of Portevin–Le Chatelier bands in cold-rolled 7Mn steel showing transformation-induced plasticity, *Int. J. Plasticity*, 103(2018), p. 188.

[29] R. Saha and R.K. Ray, Texture and grain growth characteristics in a boron added

interstitial free steel after severe cold rolling and annealing, *Mater. Sci. Eng. A*, 527(2010), No. 7-8, p. 1882.

[30] R. Saha and R.K. Ray, Effect of severe cold rolling and annealing on the development of texture, microstructure and grain boundary character distribution in an interstitial-free (IF) Steel, *ISIJ. Int.*, 48(2008), No. 7, p. 976.

[31] K. Shen and B. Duggan, Microbands and crystal orientation metastability in cold rolled interstitial-free steel, *Acta Mater.*, 55(2007), No. 4, p. 1137.

[32] L. Kestens and J.J. Jonas, Modeling texture change during the static recrystallization of interstitial-free steels, *Metall. Mater. Trans. A*, 27(1996), No. 1, p. 155.

[33] R. Every and M. Hatherly, Oriented nucleation in low-carbon steels, *Texture, Stress, Micro.*, 1(1974), No. 3, p. 183.

[34] I. Dillamore, C. Smith, and T. Watson, Oriented nucleation in the formation of annealing textures in iron, *Metal Sci. J.*, 1(1967), No. 1, p. 49.

[35] K. Verbeken, L. Kestens, and J.J. Jonas, Microtextural study of orientation change during nucleation and growth in a cold rolled ULC steel, *Scripta Mater.*, 48(2003), No. 10, p. 1457.

[36] D. Vanderschueren, N. Yoshinaga, and K. Koyama, Recrystallisation of Ti IF steel investigated with electron backscattering pattern (EBSP), *ISIJ. Int.*, 36(1996), No. 8, p. 1046.

[37] W.B. Hutchinson, Development of Textures in Recrystallization, *Metal Sci.*, 8(1974), No. 1, p. 185.

[38] J. Humphreys, G. Rohrer, and A. Rollett, *Recrystallization and Related Annealing Phenomena*, Elsevier Press, Amsterdam, 2004, p. 25.

[39] E. Nakamachi, Study of texture effect on strain localization on bcc steel sheets, *Acta Mech. Solida Sin.*, 13(2000), No. 12, p. 4.

[40] C.L. Xie and E. Nakamachi, The effect of crystallographic textures on the formability of high-strength steel sheets, *J. Mater. Process. Tech.*, 122(2002), No. 1, p. 104.

中图分类号：TG142

二级学科名称: 材料加工工程 080503